





Article

Impact of Calcium Doping on the Electronic and Optical Characteristics of Strontium Hydride (SrH₂): A DFT Study

Hamza Errahoui ¹, Mohamed Karouchi ¹, Abdelkebir Ejjabli ¹ , Aymane El haji ¹, Abdelmounaim Laassouli ¹ , Omar Ait El Alia ², Salah Chaji ^{3,*} , Youssef Lachtioui ¹ and Omar Bajjou ^{1,*} 

- ¹ Laboratory of Engineering in Chemistry and Physics of Matter, Faculty of Sciences and Technics, Sultan Moulay Slimane University, BP 523, Beni Mellal 23000, Morocco; hamzaa.errahoui@gmail.com (H.E.); karouchimohamed3@gmail.com (M.K.); ejjabliabdelkebir@gmail.com (A.E.); aymane.villani@gmail.com (A.E.h.); abdelmounaim.laassouli@gmail.com (A.L.); y.lachtioui@gmail.com (Y.L.)
- ² Laboratory of the Engineering and Applied Technologies, Higher School of Technology, Sultan Moulay Slimane University, Pb 591 M'Ghila, Beni Mellal 23000, Morocco; omar.aitelalia@usms.ma
- ³ Department of Drug Science and Technology, University of Turin, Via P. Giuria 9, 10125 Turin, Italy
- * Correspondence: salah.chaji@unito.it (S.C.); bajjou.omar@gmail.com (O.B.)

Abstract: This study investigates the electronic and optical properties of calcium-doped strontium hydride (SrH₂) using first-principles density functional theory (DFT) calculations via the CASTEP code with generalized gradient approximation (GGA). We explore the impact of calcium (Ca) doping on the electronic band structure, density of states (DOS), and optical absorption spectra of SrH₂. Our results show that Ca doping significantly alters the electronic properties of SrH₂, notably increasing the indirect bandgap from 1.3 eV to 1.6 eV. The DOS analysis reveals new states near the Fermi level, primarily from Ca 3d orbitals. Moreover, the optical absorption spectra display enhanced absorption in the visible range, suggesting the potential for optoelectronic applications. This research highlights the feasibility of tuning the electronic and optical characteristics of SrH₂ through Ca doping, thus opening the way for the generation of advanced materials with tailored properties.

Keywords: CASTEP code; DFT calculations; strontium hydride; optoelectronic properties; density of states; band gap



Citation: Errahoui, H.; Karouchi, M.; Ejjabli, A.; El haji, A.; Laassouli, A.; Ait El Alia, O.; Chaji, S.; Lachtioui, Y.; Bajjou, O. Impact of Calcium Doping on the Electronic and Optical Characteristics of Strontium Hydride (SrH₂): A DFT Study. *Atoms* **2024**, *12*, 55. <https://doi.org/10.3390/atoms12110055>

Academic Editor: Yew Kam Ho

Received: 13 September 2024

Revised: 19 October 2024

Accepted: 25 October 2024

Published: 29 October 2024



Copyright: © 2024 by the authors. Licensee MDPI, Basel, Switzerland. This article is an open access article distributed under the terms and conditions of the Creative Commons Attribution (CC BY) license (<https://creativecommons.org/licenses/by/4.0/>).

1. Introduction

Alkaline earth hydrides (AH₂) are considered promising candidates for hydrogen energy and thermal energy storage applications [1,2]. Among them, heavy alkaline earth hydrides (HAEHs), particularly those of calcium (Ca), strontium (Sr), and barium (Ba), have gained great interest due to their promising potential for hydrogen storage applications [3], fuel cells [4], and thermal energy storage. This is mainly attributed to their exceptional ionic conductivity and favorable thermal stability [5,6].

The chemistry of heavy alkaline earth hydrides (HAEHs) was initially explored in 1935 [7], when it was discovered that these compounds crystallize in an orthorhombic crystal structure with the Pnma space group. Despite this breakthrough, the exact atomic positions of hydrogen within these structures remained uncertain. For instance, the well-known hydrogen source, hydrolith (CaH₂), crystallizes in the cotunnite structure (Pnma) under ambient conditions [8]. Subsequent studies by Bergsma and Loopstra [9] provided optimized crystal structures for CaD₂ and CaH₂ through neutron diffraction, successfully identifying the correct positions of hydrogen atoms within these compounds. Further investigations utilizing neutron diffraction and nuclear magnetic resonance (NMR) studies on CaD₂ and CaH₂ refined the hydrogen atomic positions within these structures [10]. Additionally, techniques such as inelastic neutron scattering (INS) [11] and neutron vibrational spectroscopy [12] were employed to determine the crystal structures of calcium hydride and deuteride. Neutron diffraction studies of strontium deuteride (SrD₂), conducted by

Brese et al. in 1990 [13], revealed significantly different hydrogen positions, which were later corroborated and refined by Sichla and Jacobs [14].

Alkaline earth metal hydrides continue to be regarded as promising materials for hydrogen storage and optoelectronic applications. Strontium hydride (SrH_2) has drawn attention due to its favorable thermodynamic properties, high hydrogen storage capacity, and wide bandgap. However, the wide bandgap of pristine SrH_2 limits its potential in optoelectronics, especially in the visible-light region. Doping with suitable elements has therefore emerged as an effective strategy to modify the electronic structure and enhance the optical properties of various materials.

Calcium (Ca), an alkaline earth metal with ionic radii and an electronic configuration like that of Sr, has emerged as a promising candidate for doping strontium hydride (SrH_2). Previous research on calcium-doped strontium titanate (SrTiO_3) has demonstrated the effectiveness of Ca doping in altering the electronic structure and enhancing the photocatalytic activity of the material. In order to gain further insight, a comprehensive theoretical investigation utilizing density functional theory (DFT) was undertaken to assess the influence of Ca doping on the electronic and optical properties of SrH_2 .

Numerous experimental and theoretical investigations have been conducted to elucidate the structural and electronic properties of alkaline earth metal hydrides. First-principles studies by El-Gridani on CaH_2 [15,16], SrH_2 [17], and BaH_2 [18], utilizing the Hartree–Fock or pseudopotential methods within the framework of the CRYSTAL95 program, confirmed earlier results. Additionally, Smithson [19] employed density functional theory (DFT)-based methods to investigate the stability and electronic structure of various metal hydrides.

The aim of the present contribution is to thoroughly elucidate the effects of Ca doping on the electronic band structure, density of states, absorption coefficient, dielectric function, and other pertinent optical properties of SrH_2 . This study will contribute to a deeper understanding of the fundamental properties of doped SrH_2 and facilitate its prospective integration into applications in optoelectronics and energy-related fields.

2. Results and Discussion

2.1. Electronic Properties (Band Structure and Density of States)

A comparative analysis of the band structure and density of states (DOS) was conducted for both the pristine SrH_2 and the Ca-doped SrH_2 materials. The band structure analysis elucidates the impacts of calcium doping on the electronic band dispersion and energy gaps, which are crucial for understanding alterations in electronic behavior [20,21]. Furthermore, the DOS analysis reveals the distribution of electronic states across various energy levels, thereby offering insights into the impact of doping on the material's electronic density. In light of these analyses, a more profound comprehension of SrH_2 's electronic properties and prospective applications can be attained while highlighting the impact of doping on its electronic characteristics. The calculated electronic band structures and DOS for both pristine and Ca-doped SrH_2 are illustrated in Figures 1a and 1b, respectively. Pristine SrH_2 exhibits an indirect band gap of 1.3 eV at the H-G point. Following Ca doping, the band gap increases to 1.6 eV, resulting in a decrease in the material's conductivity. This increase in the band gap is attributed to the introduction of Ca 3d states above the valence band maximum (VBM) of SrH_2 , as indicated by the DOS plots.

Figure 2a–c presents the total and partial density of states (DOS) for both pristine and Ca-doped SrH_2 . Calcium doping induces significant changes in the electronic structure of SrH_2 , which are particularly evident in the DOS analysis. The total DOS for Ca-doped SrH_2 reveals pronounced peaks in both the valence and conduction bands compared with pure SrH_2 . The valence band, which is primarily influenced by the s-orbital states of hydrogen, exhibits notable peaks between -6 eV and -4 eV, which remain relatively unaffected by doping. In contrast, the conduction band shows a series of new prominent peaks between 4 eV and 8 eV, which are predominantly due to the contributions from the d-orbitals of the strontium and calcium atoms. The introduction of these additional states enhances the

material’s capacity for photon absorption at energies corresponding to these peaks, resulting in improved optical absorption in the visible and near-visible spectrum. Consequently, the doped material may exhibit enhanced optoelectronic properties, rendering it more suitable for applications in devices such as solar cells or photodetectors, where effective light absorption is essential.

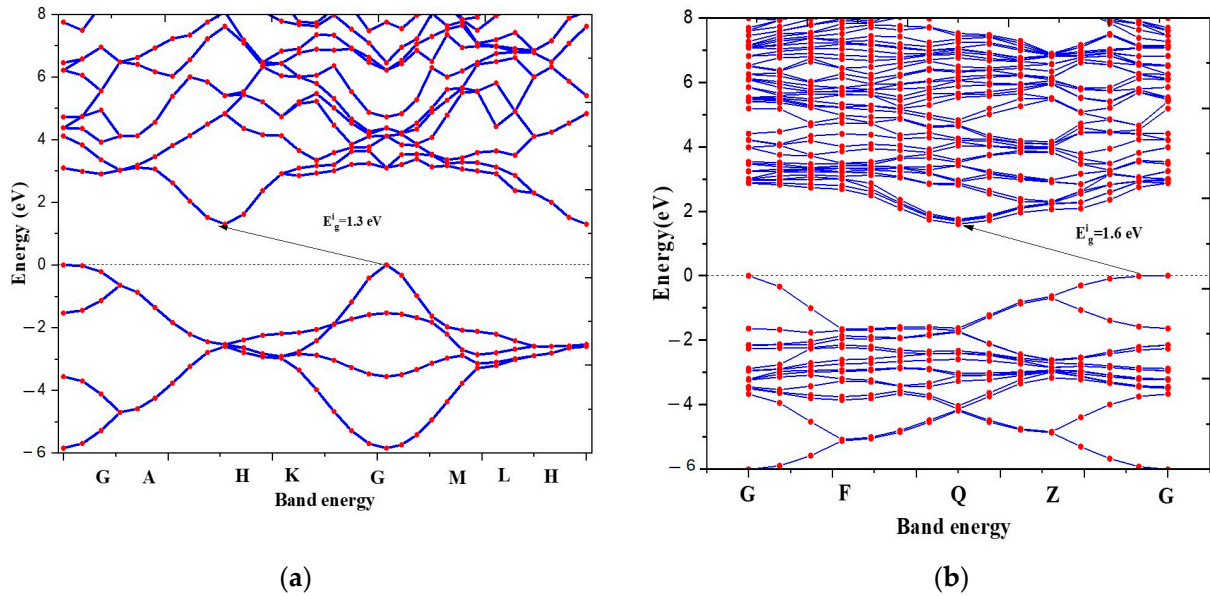


Figure 1. Band structures of (a) pristine and (b) Ca-doped SrH₂.

2.2. Optical Properties

2.2.1. Dielectric Function and Complex Refractive Index

The frequency-dependent behavior of different optical parameters of a material as a function of the energy of an incident photon ($E = h\nu$) is characterized by the material’s optical properties. A fundamental tool for analyzing this response is the frequency-dependent complex dielectric function $\epsilon(\omega)$, which provides essential insights into a range of optical behaviors. The $\epsilon(\omega)$ function is mathematically defined by the equation presented below [22,23]:

$$\epsilon(\omega) = \epsilon_1(\omega) + i\epsilon_2(\omega) \tag{1}$$

Keeping in mind that alterations in the electronic states directly impact the material’s optical response, the electronic band structure of a material is intrinsically linked to its dielectric function. The imaginary part of the dielectric function $\epsilon_2(\omega)$, which is associated with the material’s absorption properties, can be determined using the equation below [23,24]:

$$\epsilon_2(\omega) = \left(\frac{\hbar^2 e^2}{\pi m^2 \omega^2} \right) \sum_{c,v} \int d^3k \langle c_k | \hat{p}^\alpha | v_k \rangle \langle v_k | \hat{p}^\beta | c_k \rangle \times \delta(\epsilon_{c_k} - \epsilon_{v_k} - \omega) \tag{2}$$

The momentum matrix element between the band states α and β within the crystal momentum k is denoted by \hat{p} . In this context, the crystal wave functions c_k and v_k correspond to the conduction and valence bands, respectively, with k representing the crystal wave vector. $\epsilon_1(\omega)$ can be obtained from $\epsilon_2(\omega)$ using the Kramers–Kronig relation, as expressed by the equation below [25,26]:

$$\epsilon_1(\omega) = 1 + \frac{\pi}{2} p \int_0^\infty \frac{\omega' \epsilon_2(\omega')}{(\omega')^2 - \omega^2} d\omega' \tag{3}$$

where p denotes the integral’s primary value.

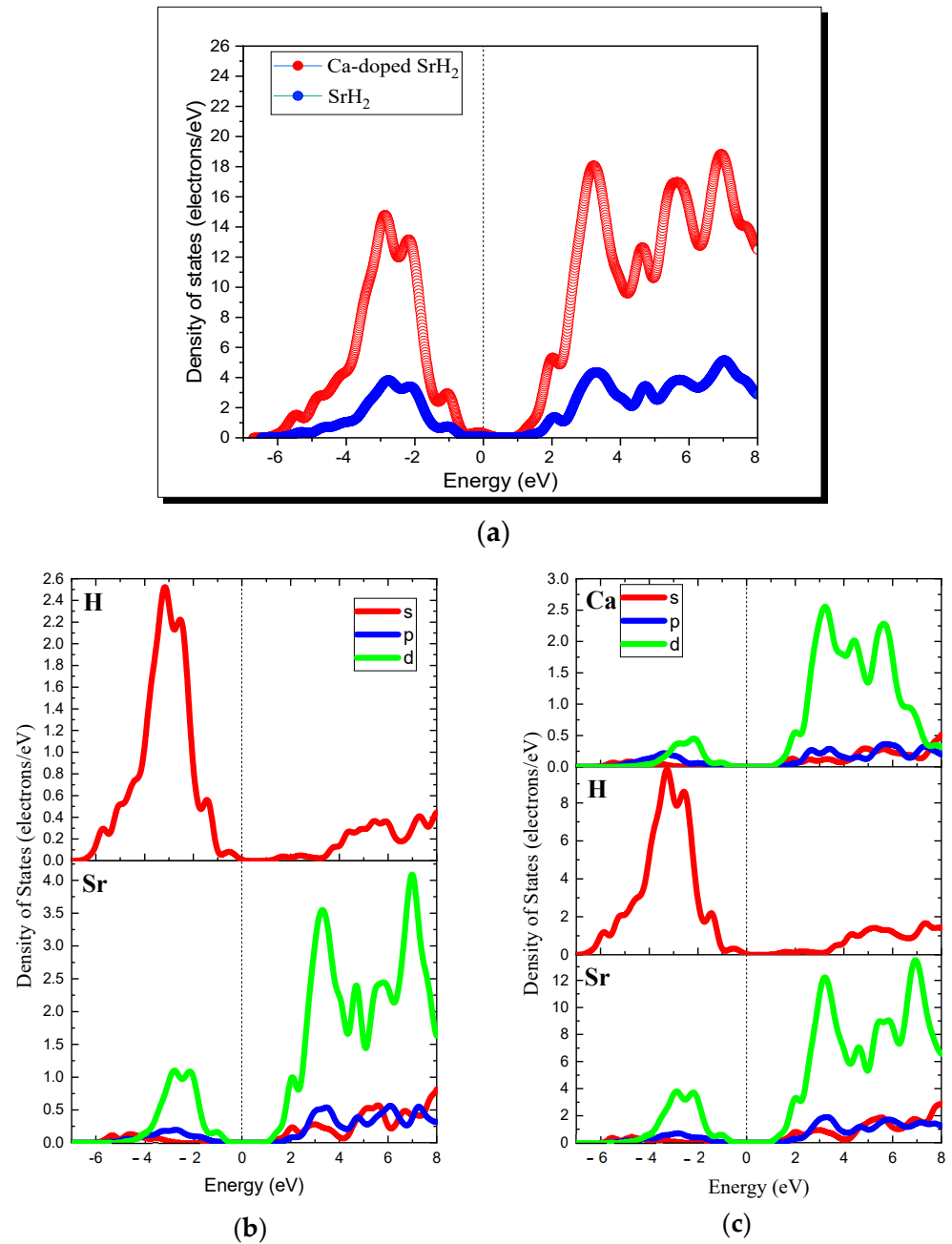


Figure 2. (a) Total DOS of pristine and Ca-doped SrH₂, partial DOS of (b) pristine SrH₂ and (c) Ca-doped SrH₂.

The optical properties were ultimately derived from the dielectric tensor values obtained through electronic structure calculations. $\epsilon_1(\omega)$, plotted on the vertical axis in Figure 3a at $\omega = 0$, represents the static values of $\epsilon_1(\omega)$. As shown in Figure 3a, the static values of $\epsilon_1(0)$ are approximately 5.01 for pristine SrH₂ and 5.12 for Ca-doped SrH₂. The spectra for both the pristine and the Ca-doped SrH₂ display a similar pattern, with slight anisotropy reflected in variations in the peak height and position. Both materials exhibit reflectivity for high-energy photons, as $\epsilon_1(\omega)$ becomes negative at approximately 9.87 eV for the pristine SrH₂ and 9.9 eV for the Ca-doped SrH₂. For crystalline materials, the electronic properties are predominantly characterized by $\epsilon_2(\omega)$, which is closely related to photon absorption phenomena. The calculated spectra of $\epsilon_2(\omega)$ for both the pristine and the Ca-doped SrH₂ are shown in Figure 3b. The threshold values of $\epsilon_2(\omega)$, calculated using the GGA-PBE approximation, reveal that the first peaks in the spectra occur at ap-

proximately 4.80 eV for the pristine SrH₂ and 4.72 eV for the Ca-doped SrH₂. These peaks arise from electronic transitions between the valence and conduction bands. The maximum values of $\epsilon_2(\omega)$ are observed at around 4.72 eV for both compounds. Beyond this point, the spectra for both materials show a decline as the energy level increases. The electronic band structures indicate that these materials exhibit an indirect band gap, leading to indirect optical transitions between the VBM and the CBM. The initial transition occurs in the G-H direction within the band structure.

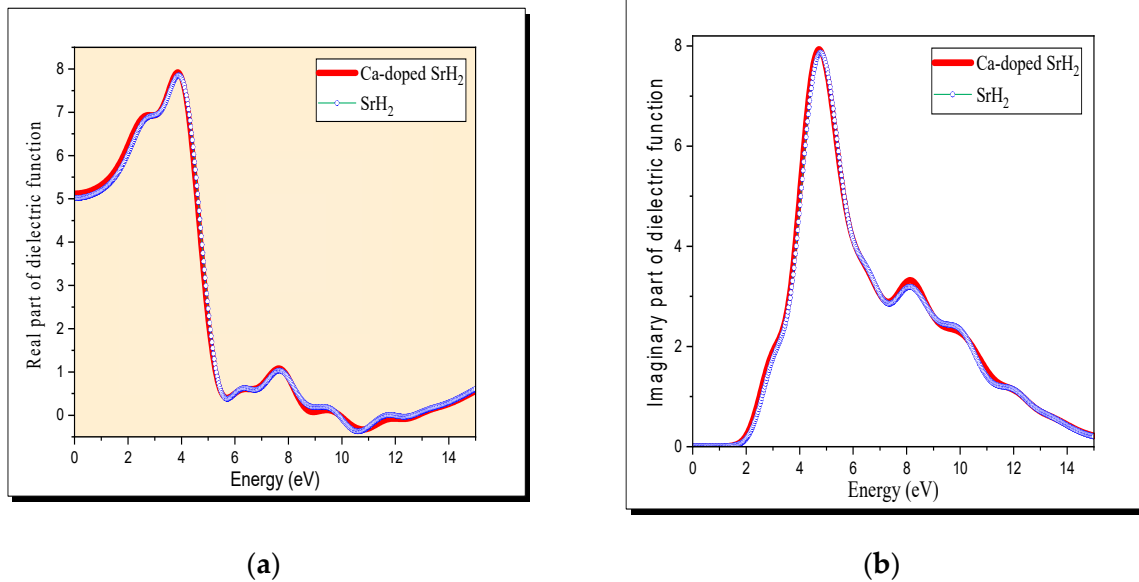


Figure 3. (a) Real part and (b) imaginary part of the dielectric function of pristine SrH₂ and Ca-doped SrH₂.

All other optical parameters, including the absorption coefficient, energy loss function, reflectivity, extinction coefficient, and refractive index, can be derived from the dielectric constants. The refractive index $n(\omega)$ of the materials studied in this study can be calculated using the following relation, which incorporates the computed values of $\epsilon_1(\omega)$ and $\epsilon_2(\omega)$ of the dielectric function [27,28]:

$$n(\omega) = \frac{1}{\sqrt{2}} \left[\sqrt{\epsilon_1^2(\omega) + \epsilon_2^2(\omega)} + \epsilon_1(\omega) \right]^{\frac{1}{2}} \quad (4)$$

The static refractive index $n(0)$, which is the refractive index at the zero-frequency limit, can be determined using the static dielectric function with the following formula [26,29]:

$$n(0) = \sqrt{\epsilon_1(0)} \quad (5)$$

The extinction coefficient $k(\omega)$ can be determined by utilizing the calculated values of $\epsilon_1(\omega)$ and $\epsilon_2(\omega)$ for the two studied materials using the following relation [24,30]:

$$k(\omega) = \frac{1}{\sqrt{2}} \left[\sqrt{\epsilon_1^2(\omega) + \epsilon_2^2(\omega)} - \epsilon_1(\omega) \right]^{\frac{1}{2}} \quad (6)$$

The calculated values of $k(\omega)$ and $n(\omega)$ for the compounds are crucial for analyzing the complex refractive index $N(\omega) = n(\omega) + ik(\omega)$ [24], which characterizes the propagation of electromagnetic waves within a material. A comprehensive understanding of $n(\omega)$ is essential for assessing the potential applications of optical materials in various devices. For instance, materials suitable for photovoltaic systems require high optical conductivity, a high absorption coefficient, low emissivity, and a high refractive index. The spectra of

$n(\omega)$ and $k(\omega)$, calculated using the GGA-PBE approximation, are presented in Figure 4a,b for both the pristine SrH₂ and the Ca-doped SrH₂. The static refractive index $n(0)$ values are approximately 2.24 and 2.26 for the pristine SrH₂ and the Ca-doped SrH₂, respectively. The maximum values of $n(\omega)$ are 2.91 for the pristine SrH₂ and 2.92 for the Ca-doped SrH₂. A comparable trend can be observed between $\varepsilon_1(\omega)$ and $n(\omega)$, as illustrated in Figures 3a and 4a. Both spectra display an initial peak at low photon energies, suggesting strong interaction with incident photons at these energy levels. This peak is followed by a steady decline in both coefficients, which can be attributed to fluctuations in the material's response as the photon energy increases. This behavior underscores the relationship between $\varepsilon(\omega)$ and $n(\omega)$ defining the optical properties of the material. Similarly, $k(\omega)$ and $\varepsilon_2(\omega)$ exhibit comparable profiles, as shown in Figures 3b and 4b. Both $k(\omega)$ and $\varepsilon_2(\omega)$ begin at a specific threshold energy. These threshold energies are approximately 1.39 eV for the pristine SrH₂ and 0.61 eV for the Ca-doped SrH₂. The maximum values of $k(\omega)$, denoted as $k_{max}(\omega)$, are 1.6880 for the pristine SrH₂ and 1.6881 for the Ca-doped SrH₂. After reaching these peak values, the extinction coefficient spectra $k(\omega)$ gradually decline toward unity.

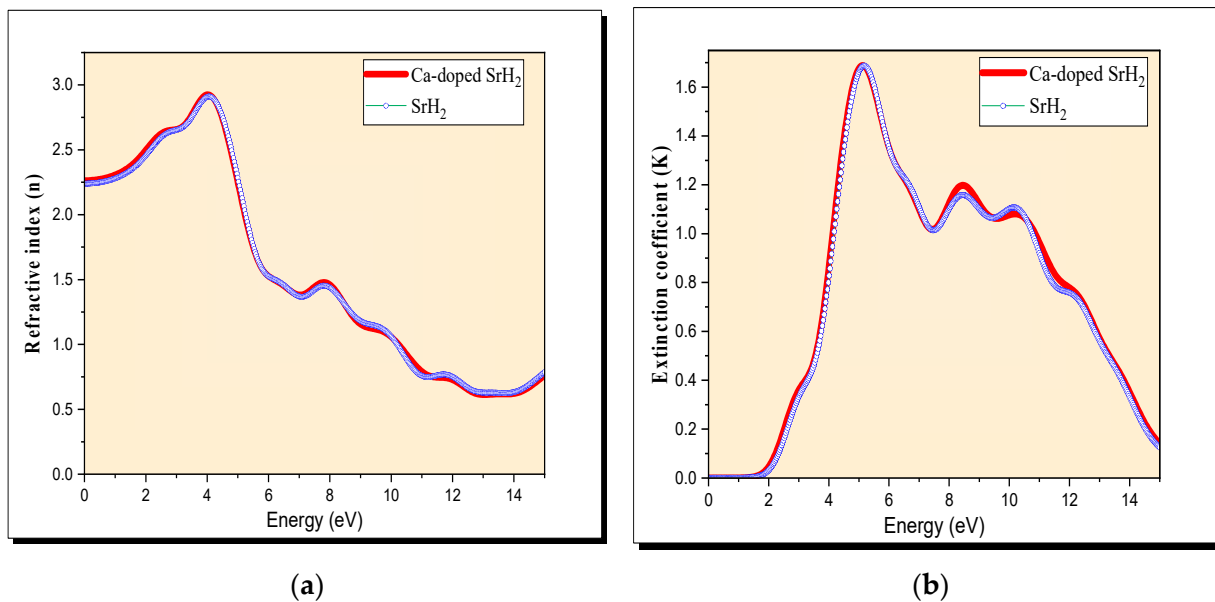


Figure 4. (a) Refractive index and (b) extinction coefficient of the dielectric function of pristine SrH₂ and Ca-doped SrH₂.

2.2.2. Absorption Coefficient, Reflectivity, Loss Function, and Conductivity

To explore the effect of Ca doping on the optical properties of SrH₂ in greater detail, the absorption coefficient was calculated. This coefficient, which reflects the material's ability to absorb light at different photon energies, was derived using the previously computed values of the real $\varepsilon_1(\omega)$ and imaginary $\varepsilon_2(\omega)$ components of the dielectric function for both pristine and Ca-doped SrH₂. The absorption coefficient $\alpha(\omega)$ can be expressed using the following relation [23]:

$$\alpha(\omega) = \sqrt{2}\omega \left[\sqrt{\varepsilon_1^2(\omega) + \varepsilon_2^2(\omega)} - \varepsilon_1(\omega) \right]^{\frac{1}{2}} \quad (7)$$

Figure 5a illustrates the calculated absorption coefficient spectra for both the pristine and the Ca-doped SrH₂. As expected, the absorption edge for the Ca-doped SrH₂ shifted toward lower energy values compared with the pristine material. This redshift in the absorption edge signifies an enhanced ability of the Ca-doped system to absorb photons across a wider spectral range, particularly within the visible-light spectrum. The improved

optical absorption properties of the Ca-doped SrH₂ suggest its potential as an advantageous material for various applications in solar-energy-related fields and optoelectronic devices. By broadening the absorption spectrum, Ca-doped SrH₂ can increase the efficiency of light absorption, making it more suitable for energy-related applications that require effective photon utilization. Calculations indicate that both the pristine and the Ca-doped SrH₂ exhibit transparency below their energy band gaps, as demonstrated in Figure 5a. This transparency occurs because the energy of incident photons is insufficient to excite electrons from the valence band to the conduction band. The absorption spectra also reveal anisotropy in both the pristine and the Ca-doped SrH₂, reflecting the directional dependence of the absorption coefficient. The latter is significantly affected by the photon frequency, as this determines the electron transitions from the valence band (VB) to the conduction band (CB). Across the entire energy range from 0 to 14 eV, the absorption coefficient of pristine SrH₂ is higher than that of Ca-doped SrH₂, indicating that Ca doping slightly reduces the material's absorption capacity. Despite this reduction, both materials exhibit strong absorption in the UV region, suggesting their suitability for optoelectronic applications in this range. As highlighted in Figure 5a, the maximum absorption coefficient values for the pristine SrH₂ and Ca-doped SrH₂ are both observed in the UV region, at approximately 10.46 eV and 10.35 eV, respectively. The maximum absorption coefficients are approximately $1.82 \times 10^5 \text{ cm}^{-1}$ for the pristine SrH₂ and $1.83 \times 10^5 \text{ cm}^{-1}$ for the Ca-doped SrH₂. These findings underscore the potential of both the pristine and the Ca-doped SrH₂ for application in UV optoelectronic devices, where their strong absorption properties can be effectively utilized. The calculated values of the complex dielectric function $\epsilon(\omega)$ can also be utilized to determine the frequency-dependent reflectivity $R(\omega)$. $R(\omega)$ is an important optical property, particularly for assessing the material's ability to reflect incident light at various frequencies. This parameter can be determined using the formula below [23,24]:

$$R(\omega) = \left| \frac{\sqrt{\epsilon(\omega) - 1}}{\sqrt{\epsilon(\omega) + 1}} \right|^2 \quad (8)$$

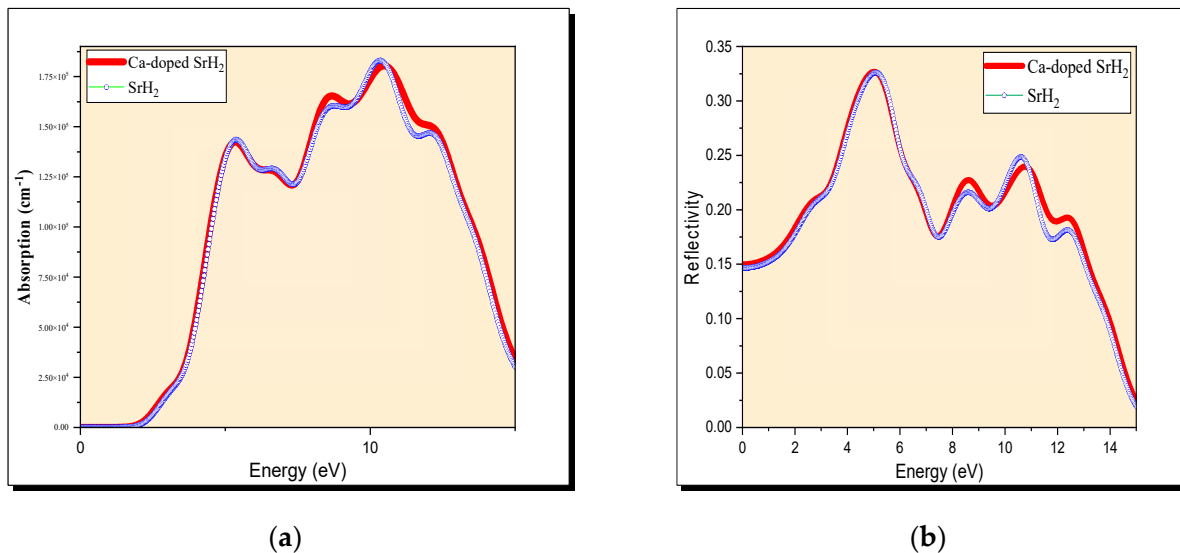


Figure 5. (a) Absorption and (b) reflectivity of pristine SrH₂ and Ca-doped SrH₂.

Figure 5b illustrates the frequency-dependent reflectivity spectra $R(\omega)$ for both the pristine SrH₂ and the Ca-doped SrH₂. As shown in the figure, the static reflectivity values (at zero frequency) are approximately 0.150 for the pristine SrH₂ and 0.146 for the Ca-doped SrH₂. The spectra reveals that the Ca-doped SrH₂ exhibits higher reflectivity compared with the pristine SrH₂ across the frequency range. The most prominent peaks in the

reflectivity spectra for both materials are observed in the energy range from 4 to 12 eV, with the $R_{max}(\omega)$ values reaching 0.3262 for the pristine SrH₂ and 0.3267 for the Ca-doped SrH₂.

The energy loss function $L(\omega)$ quantifies the energy loss experienced by high-energy electrons as they pass through a material. It provides insight into the material's interactions with fast-moving electrons and can be computed from the complex $\epsilon(\omega)$ values using the following relation [22,24]:

$$L(\omega) = \ln\left(-\frac{1}{\epsilon(\omega)}\right) \quad (9)$$

Figure 6 displays the calculated spectra $L(\omega)$ across the energy range from 0 to 14 eV. $L(\omega)$ offers significant insights into the interactions between incident photons and the material's electronic systems. It is noteworthy that a corresponding reduction in the reflectivity spectra is observed at these same energy points. The energy loss function $L(\omega)$ exhibits prominent peaks at 13.89 eV and 13.81 eV for the pristine SrH₂ and the Ca-doped SrH₂, respectively, signifying plasma resonance at these plasma frequencies.

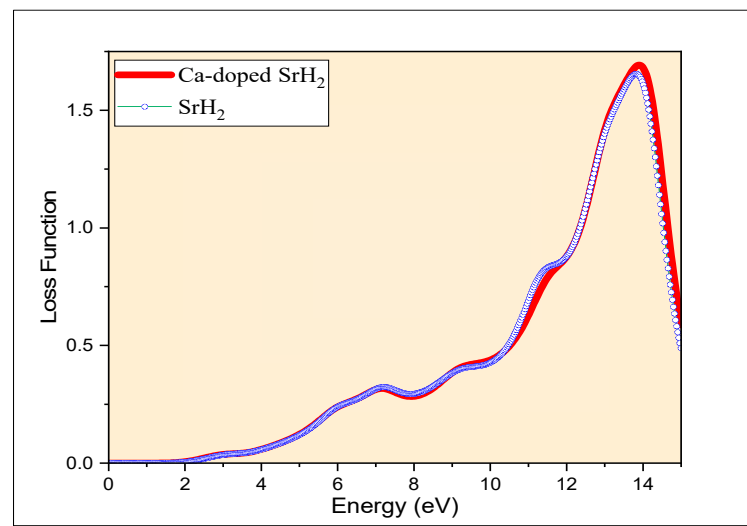


Figure 6. Loss function of pristine SrH₂ and Ca-doped SrH₂.

Figure 7a,b illustrates the real and imaginary parts of the optical conductivity σ for both the pristine SrH₂ and the Ca-doped SrH₂ across a range of energies.

In Figure 7b, the imaginary part of the conductivity reveals notable differences between the two materials. For the pristine SrH₂, the curve displays negative peaks at around 4 eV and beyond, indicating notable energy absorption or polarization effects. In contrast, the Ca-doped SrH₂ shows reduced intensity for these features, suggesting that Ca doping diminishes the absorption at these specific energy levels. It seems probable that this reduction is attributable to alterations in the electronic structure that result from doping, which effectively shift the energy levels involved in optical transitions.

Figure 7a depicts the real part of the conductivity, where distinct differences are also observed due to Ca doping. Pristine SrH₂ exhibits a sharp peak at around 4.88 eV, indicating strong conductivity at this energy. In the Ca-doped sample, this peak becomes broader and slightly less pronounced, suggesting increased scattering and a more diffusive electronic structure. Additionally, at higher energies (above 11.98 eV), the σ in the doped material is consistently lower than in the pristine sample, reflecting a decrease in the number of free carriers or available states for conduction.

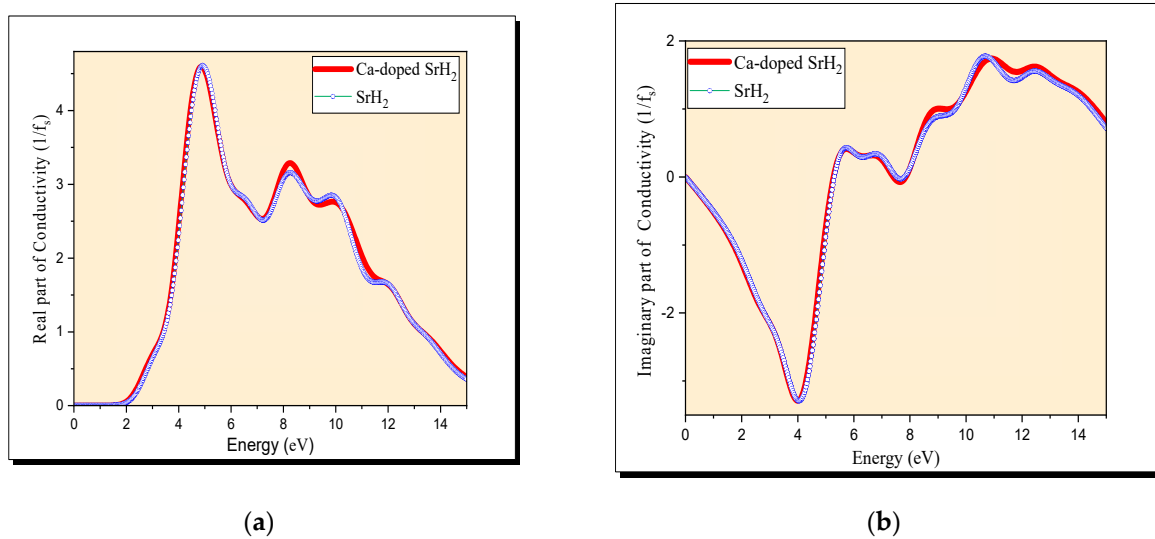


Figure 7. (a) Real part and (b) imaginary part of the conductivity of pristine SrH₂ and Ca-doped SrH₂.

3. Computational Methods

First-principles calculations were conducted using DFT within the *CASTEP* code framework [31,32]. Exchange-correlation interactions were modeled with the Perdew–Burke–Ernzerhof (PBE) functional, employing generalized gradient approximation (GGA) [33,34]. OTFG ultrasoft pseudopotentials were used to represent the interactions between ionic cores and valence electrons [24]. Plane-wave basis sets with a cutoff energy of 500 eV were applied to expand the electronic wavefunctions. Brillouin zone integrations were performed using a $6 \times 6 \times 6$ Monkhorst–Pack k-point mesh for structural optimization [35] along with electronic and optical property calculations.

The structure of SrH₂ was initially optimized until the forces on each atom were reduced to below 0.05 eV/Å. To ensure a thorough investigation of the material’s properties, the supercell of SrH₂, which adopts a hexagonal structure, was expanded by doubling the lattice parameters in both the X and Y directions before doping. Following this, one Sr atom was substituted with a Ca atom, resulting in a doping concentration of 12.5%. The electronic and optical properties of both the pristine and the Ca-doped SrH₂ were then calculated using the optimized structures. There are two distinct H[−] sites present. In the first H[−] site, H[−] is bonded to five equivalent Sr²⁺ atoms, forming HSr₅ trigonal bipyramids (Figure 8). These bipyramids share corners with twelve equivalent HSr₆ octahedra and eight equivalent HSr₅ trigonal bipyramids, edges with six equivalent HSr₅ trigonal bipyramids, and faces with six equivalent HSr₆ octahedra. The tilt angles of the corner-sharing octahedra range from 31° to 59°. In the second H[−] site, H[−] is bonded to six equivalent Sr²⁺ atoms, forming HSr₆ octahedra. These octahedra share faces with two equivalent HSr₆ octahedra and faces with six equivalent HSr₅ trigonal bipyramids. The tilt angles of the corner-sharing octahedra are 51°. Atomic positions and lattice parameters for SrH₂ are detailed in Tables 1 and 2, respectively.

Table 1. Atomic positions.

Wyckoff	Element	x	y	z
2a	H	0	0	0
2c	Sr	2/3	1/3	3/4
2d	H	2/3	1/3	1/4

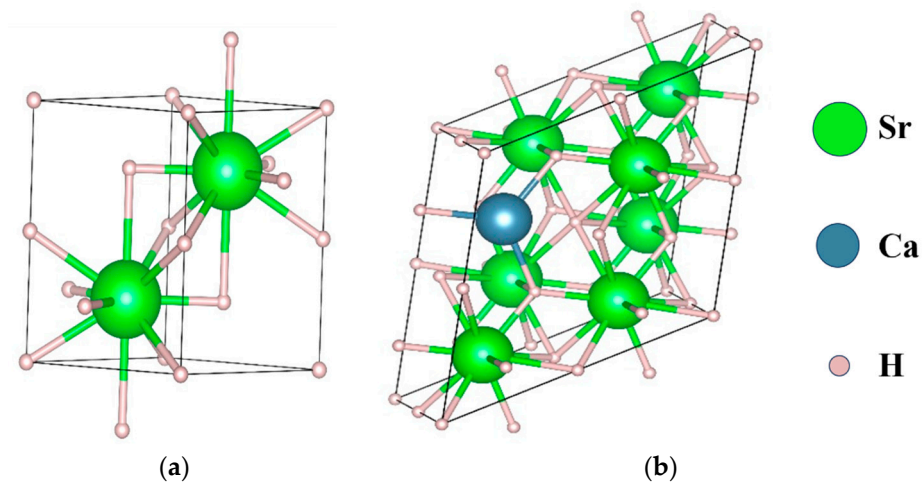


Figure 8. Crystal structures of (a) pristine and (b) Ca-doped SrH₂.

Table 2. Lattice parameters.

<i>a</i>	4.12 Å
<i>b</i>	4.12 Å
<i>c</i>	5.68 Å
α	90.00°
β	90.00°
γ	120.00°
Volume	83.51 Å ³

4. Conclusions

This research presents a comprehensive investigation into the electronic and optical properties of both the pristine and the Ca-doped SrH₂ through the utilization of first-principles calculations based on DFT. The findings demonstrate that Ca doping notably alters the electronic structure of SrH₂; this results in an increase in the band gap from 1.3 eV to 1.6 eV. This widening of the band gap corresponds to a reduction in intrinsic conductivity, as evidenced by the decreased real part of the optical conductivity at higher energies. Furthermore, the introduction of Ca enhances the density of states in the conduction band, shifting the absorption edge to lower energies and improving photon absorption efficiency in the visible spectrum. The doping effect is evidenced by a slight increase in the static dielectric constant and refractive index, which reflects altered optical behavior. The enhanced reflectivity and absorption characteristics indicate that Ca-doped SrH₂ may exhibit superior performance in the UV–visible range. These findings indicate that Ca-doped SrH₂ is a promising candidate for optoelectronic applications, such as solar cells and photodetectors. Hence, it seems reasonable to state that the introduction of Ca has proven to be an effective method for modifying the electronic and optical properties of SrH₂ in a way that broadens its potential applications in advanced material technologies.

Author Contributions: Conceptualization, O.B. and A.L.; methodology, H.E. and A.E.; software, H.E., A.E.h. and M.K.; validation, O.B., Y.L. and S.C.; formal analysis, H.E. and O.A.E.A.; investigation, H.E. and O.A.E.A.; resources, H.E. and M.K.; data curation, H.E. and A.E.h.; writing—original draft preparation, H.E. and M.K.; writing—review and editing, A.E. and S.C.; visualization, A.L.; supervision, O.B. All authors have read and agreed to the published version of the manuscript.

Funding: This research received no external funding.

Data Availability Statement: The original contributions presented in the study are included in the article. Further inquiries can be directed to the corresponding author.

Conflicts of Interest: The authors declare that the research was conducted in the absence of any commercial or financial relationships that could be construed as a potential conflict of interest.

References

1. Sadhasivam, T.; Sterlin Leo Hudson, M.; Pandey, S.K.; Bhatnagar, A.; Singh, M.K.; Gurunathan, K.; Srivastava, O.N. Effects of Nano Size Mischmetal and Its Oxide on Improving the Hydrogen Sorption Behaviour of MgH_2 . *Int. J. Hydrogen Energy* **2013**, *38*, 7353–7362. [[CrossRef](#)]
2. Oumellal, Y.; Zaïdi, W.; Bonnet, J.-P.; Cuevas, F.; Latroche, M.; Zhang, J.; Bobet, J.-L.; Rougier, A.; Aymard, L. Reactivity of TiH_2 Hydride with Lithium Ion: Evidence for a New Conversion Mechanism. *Int. J. Hydrogen Energy* **2012**, *37*, 7831–7835. [[CrossRef](#)]
3. George, L.; Saxena, S.K. Structural Stability of Metal Hydrides, Alanates and Borohydrides of Alkali and Alkali- Earth Elements: A Review. *Int. J. Hydrogen Energy* **2010**, *35*, 5454–5470. [[CrossRef](#)]
4. Rowberg, A.J.E.; Weston, L.; Van de Walle, C.G. Ion-Transport Engineering of Alkaline-Earth Hydrides for Hydride Electrolyte Applications. *Chem. Mater.* **2018**, *30*, 5878–5885. [[CrossRef](#)]
5. Tang, L.; Wang, Y.; Li, J. The Graphene/Nucleic Acid Nanobiointerface. *Chem. Soc. Rev.* **2015**, *44*, 6954–6980. [[CrossRef](#)]
6. Yagyu, H.; Kato, M.; Noji, T.; Koike, Y. Synthesis of Perovskite-Type Hydrides $APdH_3$ (A = Sr, Ba) by a New Method Using CaH_2 as a H_2 -Source. *Phys. Procedia* **2013**, *45*, 109–112. [[CrossRef](#)]
7. Egbewale, B.E.; Mabayoje, V.O.; Muhibi, M.A.; Mustapha, A.F.; Akinleye, C.A. Screening Outcomes of Hepatitis B and E among HIV Patients on HAART in Osogbo, SouthWestern Nigeria. *World J. AIDS* **2016**, *06*, 205–217. [[CrossRef](#)]
8. Tse, J.S.; Klug, D.D.; Desgreniers, S.; Smith, J.S.; Flacau, R.; Liu, Z.; Hu, J.; Chen, N.; Jiang, D.T. Structural phase transition in CaH_2 at high pressures. *Phys. Rev. B* **2007**, *75*, 134108. [[CrossRef](#)]
9. Bergsma, J.; Loopstra, B.O. The Crystal Structure of Calcium Hydride. *Acta Crystallogr.* **1962**, *15*, 92–93. [[CrossRef](#)]
10. Andresen, A.F.; Maeland, A.J.; Slotfeldt-Ellingsen, D. Calcium Hydride and Deuteride Studied by Neutron Diffraction and NMR. *J. Solid State Chem.* **1977**, *20*, 93–101. [[CrossRef](#)]
11. Colognesi, D.; Barrera, G.; Ramirez-Cuesta, A.J.; Zoppi, M. Hydrogen Self-Dynamics in Orthorhombic Alkaline Earth Hydrides through Incoherent Inelastic Neutron Scattering. *J. Alloys Compd.* **2007**, *427*, 18–24. [[CrossRef](#)]
12. Wu, H.; Zhou, W.; Udovic, T.J.; Rush, J.J.; Yildirim, T. Structure and Vibrational Spectra of Calcium Hydride and Deuteride. *J. Alloys Compd.* **2007**, *436*, 51–55. [[CrossRef](#)]
13. Brese, N.E.; O’Keeffe, M.; Von Dreele, R.B. Synthesis and Crystal Structure of SrD_2 and $SrND$ and Bond Valence Parameters for Hydrides. *J. Solid State Chem.* **1990**, *88*, 571–576. [[CrossRef](#)]
14. Ejjabli, A.; Karouchi, M.; Errahoui, H.; Bajjou, O.; Guerroum, J.; Elhajji, A.; Rahmani, K.; Lachtioui, Y. Electronic and Optical Properties of Double Perovskite Oxide $LaFeWO_6$: A Theoretical Understanding from DFT Calculations. *E3S Web of Conferences* **2024**, *582*, 02001. [[CrossRef](#)]
15. El Gridani, A.; El Mouhtadi, M. Electronic and Structural Properties of CaH_2 : An Ab Initio Hartree–Fock Study. *Chem. Phys.* **2000**, *252*, 1–8. [[CrossRef](#)]
16. El Gridani, A.; El Mouhtadi, M. Electronic and Structural Properties of CaH_2 : A Pseudopotential Study. *J. Mol. Struct. THEOCHEM* **2000**, *532*, 183–193. [[CrossRef](#)]
17. El Gridani, A.; Drissi El Bouzaidi, R.; El Mouhtadi, M. Elastic, Electronic and Crystal Structure of SrH_2 by the Method of Pseudopotentials. *J. Mol. Struct. THEOCHEM* **2000**, *531*, 193–210. [[CrossRef](#)]
18. El Gridani, A.; Drissi El Bouzaidi, R.; El Mouhtadi, M. Elastic, Electronic and Crystal Structure of BaH_2 : A Pseudopotential Study. *J. Mol. Struct. THEOCHEM* **2002**, *577*, 161–175. [[CrossRef](#)]
19. Smithson, H.; Marianetti, C.A.; Morgan, D.; Van der Ven, A.; Predith, A.; Ceder, G. First-Principles Study of the Stability and Electronic Structure of Metal Hydrides. *Phys. Rev. B* **2002**, *66*, 144107. [[CrossRef](#)]
20. Archi, M.; Al-hattab, M.; Bajjou, O.; Moulaoui, L.; Rahmani, K.; Elhadadi, B. The Effect of Doping/Dual-Doping with Nitrogen and Silicon on the Structural, Electronic, and Optical Properties of Graphene: First-Principles Study. *J. Nanoparticle Res.* **2024**, *26*, 138. [[CrossRef](#)]
21. Laassouli, A.; Bajjou, O.; Lachtioui, Y.; Najim, A.; Moulaoui, L.; Rahmani, K. DFT Investigation on the Electronic and Optical Properties of Br-Doped $CH_3NH_3 SnI_3$ Perovskite. In Proceedings of the 2023 3rd International Conference on Innovative Research in Applied Science, Engineering and Technology (IRASET), Mohammedia, Morocco, 18–19 May 2023; IEEE: Piscataway, NJ, USA, 2023; pp. 1–6.
22. Archi, M.; Bajjou, O.; Moulaoui, L.; Najim, A.; Karouchi, M.; Rahmani, K.; El haddadi, B. Electronic and Optical Properties of Different Concentrations of Ga Doped ZnO: CASTEP Study. In Proceedings of the 2023 3rd International Conference on Innovative Research in Applied Science, Engineering and Technology (IRASET), Mohammedia, Morocco, 18–19 May 2023; IEEE: Piscataway, NJ, USA, 2023; pp. 1–7.

23. Karouchi, M.; Bajjou, O.; Jabraoui, H.; Ejjabli, A.; Archi, M.; Moulaoui, L.; Rahmani, K.; Lachtioui, Y. Increasing Electro-Optical Properties of Perovskite FAPbI_3 Under the Effect of Doping by Sn. In Proceedings of the 2023 3rd International Conference on Innovative Research in Applied Science, Engineering and Technology (IRASET), Mohammedia, Morocco, 18–19 May 2023; IEEE: Piscataway, NJ, USA, 2023; pp. 1–7.
24. Ejjabli, A.; Karouchi, M.; Al-Hattab, M.; Bajjou, O.; Rahmani, K.; Lachtioui, Y. Investigation of Lead-Free Halide $\text{K}_2\text{AgSbBr}_6$ Double Perovskite's Structural, Electronic, and Optical Properties Using DFT Functionals. *Chem. Phys. Impact* **2024**, *9*, 100656. [[CrossRef](#)]
25. King-smith, R.D.; Vanderbilt, D. A first-principles pseudopotential investigation of ferroelectricity in barium titanate. *Ferroelectrics* **1992**, *136*, 85–94. [[CrossRef](#)]
26. Li, W.; Landis, C.M.; Demkov, A.A. Domain morphology and electro-optic effect in Si-integrated epitaxial BaTiO_3 films. *Phys. Rev. Mater.* **2022**, *6*, 095203. [[CrossRef](#)]
27. Munir, S.; Butt, M.K.; Aldaghfag, S.A.; Misbah, Y.; Yaseen, M.; Nasarullah; Nazar, M.; Somaily, H.H. First-principles Calculations to Investigate Emerging Double Perovskites K_2NaMoX_6 ($X=\text{Cl, I}$) Compounds for Magnetic and Optoelectronic Applications. *Phys. B Condens. Matter* **2022**, *645*, 414252. [[CrossRef](#)]
28. Ma, Y.; Chen, H.; Pan, F.; Chen, Z.; Ma, Z.; Lin, X.; Zheng, F.; Ma, X. Electronic structures and optical properties of Fe/Co-doped cubic BaTiO_3 ceramics. *Ceram. Int.* **2019**, *45*, 6303–6311. [[CrossRef](#)]
29. Chen, Q.; Zhou, L.; Zhang, J.; Chen, D.; Zhu, W.; Xi, H.; Zhang, J.; Zhang, C.; Hao, Y. Recent progress of wide bandgap perovskites towards two-terminal perovskite/silicon tandem solar cells. *Nanomaterials* **2024**, *14*, 202. [[CrossRef](#)]
30. Karouchi, M.; Ejjabli, A.; Bajjou, O.; Guerroum, J.; Al-Hattab, M.; Basyooni, M.; Kabatas, M.A.; Rahmani, K.; Lachtioui, Y. Investigating the Structural, Electronic, and Optical Properties of the Novel Double Perovskite K_2AgBiI_6 Using DFT. *Front. Mater.* **2024**, *11*, 1448400. [[CrossRef](#)]
31. Clark, S.J.; Segall, M.D.; Pickard, C.J.; Hasnip, P.J.; Probert, M.J.; Refson, K.; Payne, M.C. First principles methods using CASTEP. *Z. Für Krist. Cryst. Mater.* **2005**, *220*, 567–570. [[CrossRef](#)]
32. Munio, A.A.Z.; Liboon, A.Q., Jr.; Lagud, Y.J.; Patayon, U.B.; Pido, A.A.G.; Karouchi, M.; Ambolode, L.C.C., II. A Density Functional Theory Study on the Interaction of Cellulose Biopolymer and Atomic Arsenic. *Solid State Phenomena* **2023**, *352*, 39–46. [[CrossRef](#)]
33. Segall, M.D.; Lindan, P.J.D.; Probert, M.J.; Pickard, C.J.; Hasnip, P.J.; Clark, S.J.; Payne, M.C. First-Principles Simulation: Ideas, Illustrations and the CASTEP Code. *J. Phys. Condens. Matter* **2002**, *14*, 2717–2744. [[CrossRef](#)]
34. Perdew, J.P.; Burke, K.; Ernzerhof, M. Generalized Gradient Approximation Made Simple. *Phys. Rev. Lett.* **1996**, *77*, 3865–3868. [[CrossRef](#)] [[PubMed](#)]
35. Monkhorst, H.J.; Pack, J.D. Special Points for Brillouin-Zone Integrations. *Phys. Rev. B* **1976**, *13*, 5188–5192. [[CrossRef](#)]

Disclaimer/Publisher's Note: The statements, opinions and data contained in all publications are solely those of the individual author(s) and contributor(s) and not of MDPI and/or the editor(s). MDPI and/or the editor(s) disclaim responsibility for any injury to people or property resulting from any ideas, methods, instructions or products referred to in the content.